CrossMark

ORIGINAL RESEARCH PAPER

# Cyclic tensile-compressive tests on thin concrete boundary elements with a single layer of reinforcement prone to out-of-plane instability

Angelica Rosso[1] · Lisandro A. Jiménez-Roa[1] ·
João Pacheco de Almeida[1] · Aydee Patricia Guerrero Zuniga[2] ·
Carlos A. Blandón[3] · Ricardo L. Bonett[4] · Katrin Beyer[1]

**Abstract** The growing need for residential housing in Latin American countries has led to the construction of reinforced concrete buildings with wall thicknesses as low as 8–10 cm. Such walls have typically only a single layer of vertical rebars and are therefore particularly susceptible to out-of-plane failure. In order to investigate the response of the corresponding wall boundary elements, twelve reinforced concrete members with a single layer of vertical rebars were tested under tension–compression cycles. The objective was to gain insight into the parameters governing wall instability and out-of-plane failure, namely the thickness, reinforcement ratio, and eccentricity of the longitudinal rebars with respect to the member axis. This paper summarises the results of the test program, where the

✉ Katrin Beyer
  katrin.beyer@epfl.ch

  Angelica Rosso
  angelica.rosso@epfl.ch

  Lisandro A. Jiménez-Roa
  lisandro.jimenez@epfl.ch

  João Pacheco de Almeida
  joao.almeida@epfl.ch

  Aydee Patricia Guerrero Zuniga
  aydeegzu@univalle.edu.co

  Carlos A. Blandón
  carlos.blandon@eia.edu.co

  Ricardo L. Bonett
  rbonett@udem.edu.co

[1] Earthquake Engineering and Structural Dynamics Laboratory (EESD), School of Architecture, Civil and Environmental Engineering (ENAC), École Polytechnique Fédérale de Lausanne (EPFL), Station 18, 1015 Lausanne, Switzerland

[2] School of Civil Engineering, Universidad del Valle, Cali, Colombia

[3] Escuela de Ingeniería de Antioquia –E.I.A. University, Medellín, Colombia

[4] Universidad de Medellín – Udem, Medellín, Colombia

 Springer

specimens' response is analysed also at the global and local levels. The results show that the crack pattern has an important influence on the out-of-plane behaviour and the conditions leading to out-of-plane failure are described. Furthermore, the differences between members with a single layer of vertical rebars and members with two layers are discussed. The influence of the parameters considered in the experimental program is addressed, showing that sections with small thickness and large reinforcement content are more prone to out-of-plane failures. Finally, predictions given by existing models are compared to the new experimental data. The entire data set is publicly available.

# 1 Introduction

Over the last few years, the growing need of housing for low-income population in several South America countries, has led to build medium-to-high rise reinforced concrete (RC) wall structures, which represent a common solution when the land cost is high. Moreover, since the material costs are also substantial, the walls are constructed with very low thicknesses and light amount of reinforcement placed in a single layer. Several structures, with significantly thicker RC walls, were damaged after the Chile and New Zealand earthquakes of 2010 and 2011, and in several cases out-of-plane buckling of the walls, was observed (Wallace et al. 2012; Sritharan et al. 2014). In Chile and New Zealand the thickness of the walls varies typically between 15 and 25 cm (Wallace et al. 2012), while in some Latin American countries—such as Colombia—the wall thickness of new constructions can be as low as 8–10 cm (Arteta et al. 2017). It is expected that the small thickness and the single layer of vertical reinforcement make these walls particularly susceptible to out-of-plane failure.

The critical region of a RC wall susceptible to out-of-plane instability is the boundary element, and the existing models for describing the out-of-plane buckling mechanism (addressed in Sect. 1.1), assimilate it to an equivalent column axially loaded in tension and compression. Although recent tests on walls have shown that out-of-plane deformations can extend throughout a relatively large part of the wall length (Rosso et al. 2016), the boundary elements are indeed the critical wall part in which the development of the out-of-plane instability is triggered (Goodsir 1985). Previous experimental studies concentrated on boundary elements with two layers of vertical rebars (Sect. 1.2). Therefore, within a collaborative project between the École Polytechnique Fédérale de Lausanne (*EPFL*) in Switzerland and three Colombian Universities—the University of Valle, the E.I.A. University and the University of Medellin—an experimental program on twelve RC boundary elements with a single layer of vertical reinforcement was carried out at *EPFL*.

The specimens were designed to be representative of members vulnerable to out-of-plane instability within current Colombian construction practice (see Sect. 2.1). The aim of the experimental program was to investigate the influence of several parameters, namely the wall thickness, the reinforcement content, and the eccentricity of the single layer of reinforcement with respect to the member axis, on the out-of-plane response. Sections 2.2 and 2.3 describe the geometry of the specimens, the test setup, and the loading protocol. Section 3 presents the behaviour of each test unit whilst in Sects. 4 the main findings are outlined and discussed. Finally, in Sect. 5 the predictions of existing models with regard to

the critical tensile strain that causes out-of-plane failure are compared to the experimental results.

## 1.1 Existing models for out-of-plane instability

Reviews of existing models to assess out-of-plane stability of members reinforced with one or two layers of reinforcement can be found in the literature (Herrick and Kowalsky 2016; Parra 2016; Rosso et al. 2016), and in the following only the main aspects are briefly recalled. Goodsir and Paulay (Goodsir 1985; Paulay and Goodsir 1985) were the first authors to study the instability of RC walls. Paulay and Priestley (1993), a few years later, proposed a model based on axially loaded columns, pinned at the ends, representative of RC wall boundary elements in the plastic hinge regions. They formulated equilibrium in an out-of-plane configuration and derived the following stability criterion:

$$\xi_{oop,cr} = 0.5 \cdot \left(1 + 2.35\,m - \sqrt{5.53\,m^2 + 4.70\,m}\right) \leq 0.5 \tag{1}$$

where $\xi_{oop,cr}$ is the critical out-of-plane displacement normalized to the member thickness (b) triggering an out-of-plane failure, $m = \rho_{BE}f_y/f_c$ is the mechanical reinforcement ratio ($\rho_{BE}$ is the boundary element reinforcement ratio, $f_y$ is the reinforcement yield strength, and $f_c$ is the concrete compressive strength).

The height of the equivalent column $l_0$ is assumed equal to the equivalent plastic hinge length, as computed by $l_p = 0.20 \cdot l_w + 0.044 \cdot L_s$ ($l_w$ and $L_s$ are the length and the shear span of the cantilever wall respectively). Paulay and Priestley (1993) derived the following relation between the average critical tensile strain $\varepsilon_{cr}$ (over $l_0$) causing out-of-plane failure and the critical normalized out-of-plane displacement $\xi_{oop,cr}$:

$$\varepsilon_{cr} = 8\beta \left(\frac{b}{l_0}\right)^2 \xi_{oop,cr} \tag{2}$$

This equation was derived from geometrical considerations, assuming that the elongation in arc length due to wall out-of-plane deformation results from the axial increase of the equivalent column over the buckling length. To account for the location of the longitudinal reinforcement within the wall section, the parameter $\beta$ is assumed equal to 0.5 or 0.8 when the longitudinal reinforcement is placed in one or two layers respectively. Chai and Elayer (1999), using the stability criterion by Paulay and Priestley (1993), derived a phe-nomenological equation for the critical tensile strain, based on the test results of an experimental program on axially loaded double-layered RC elements. Therefore, their approach is not suitable to evaluate the out-of-plane stability of single-layered members. More recently, Parra and Moehle (Parra and Moehle 2014; Parra 2016) combined the stability criterion by Paulay and Priestley (1993) with the sinusoidal distribution of cur-vatures by Chai and Elayer (1999), further assuming that the maximum displacement occurs for a residual tensile strain of $\varepsilon_{sm} - 0.005$, where $\varepsilon_{sm}$ is the maximum tensile strain experienced in tension before the loading is reversed. Since 0.005 is typically larger than twice the yield strain of the reinforcement, it is therefore assumed that the reinforcement yields in compression when out-of-plane buckling occurs, which as shown later is not applicable for single-layered members. Moreover, the derived criterion explicitly accounts for a range of different boundary conditions (Parra and Moehle 2014):

$$\varepsilon_{cr} = \pi^2 \beta \left(\frac{b}{k \cdot l}\right)^2 \xi_{oop,cr} + 0.005 \qquad (3)$$

where $k{\cdot}l$ is the effective height involved in the buckling mechanism, e.g., $k = 0.5$ if the boundary element is considered fixed at the top and bottom.

To evaluate the accuracy of the models by Paulay and Priestley (1993) and Chai and Elayer (1999) in predicting experimental test results on thin walls and boundary elements, Herrick and Kowalsky (2016) calculated the axial strain–displacement response of past tests on two-layer boundary elements, using moment–curvature analysis and standard plastic hinge calculations. According to their approach, the model by Chai and Elayer (1999) generally estimates buckling critical tensile strains more accurately than the one by Paulay and Priestley (1993).

More recently, the out-of-plane instability was also investigated with finite element models. It was shown that such models are able to capture the entire response of the members, but the analyses are numerically complex due to the highly nonlinear geometrical and material behaviour involved in the simulation process. Boundary elements subjected to tensile-compressive loading were simulated using beam-column models (Parra 2016; Rosso et al. 2017a) and curved shell elements (Parra 2016; Rosso et al. 2017c). Using the latter type of finite elements, the first to model the behaviour of an entire wall subjected to in-plane loading were Dashti et al. (2017), then followed by other researchers (Parra 2016; Scolari 2017). These numerical tools appear to be a promising avenue for the simulation of out-of-plane response and subsequent failure.

## 1.2 Previous test campaigns on boundary elements investigating out-of-plane failure

As stated above, the boundary element of a wall can be approximated by an equivalent column subjected to tensile-compressive loads, and this idealization was assumed in several experimental programs. Most boundary element tests addressed the behaviour of walls with two layers of reinforcement and were not specifically addressed to study the out-of-plane buckling of RC members (Goodsir 1985; Miranda et al. 1990; Chai and Elayer 1999; Acevedo et al. 2010; Creagh et al. 2010; Chrysanidis and Tegos 2012; Hilson et al. 2014; Taleb et al. 2016; Welt et al. 2016). Therefore, failure often occurred not due to lateral instability, but due to concrete crushing or local rebar buckling. Only the experimental program by Menegon et al. (2015) comprised also one specimen with a single layer of longitudinal reinforcement, which was designed to be representative of Australian construction practice. The boundary element attained significant out-of-plane displacement (larger than $0.5b$), which was, however, almost fully recovered before a local failure in compression occurred due to rebar buckling.

Important findings related to the development of out-of-plane instability that were obtained from these past experimental programs are: (1) sections with large height-to-thickness ratios are prone to easily develop large out-of-plane deformations; (2) tensile strain applied prior to subsequent loading in compression is the parameter that governs the out-of-plane instability, for which several expressions have been proposed as discussed in the previous section. Lacking are experimental results on boundary elements with a single layer of longitudinal reinforcement and tests that address the influence of various parameters on the out-of-plane response, such as the reinforcement content, the bar diameter, and the eccentricity of the single layer of reinforcement with respect to the

centreline of the section. The experimental program presented in this paper attempts to provide new insights with regard to these issues.

## 2 Description of the experimental program

### 2.1 Colombian construction practice on RC wall buildings

To design the specimens of the experimental program, the blueprints of nine buildings located in the neighbourhood of Cali, the third largest city of Colombia and code-located in the 'high seismic zone', were analysed, and the main properties of around 800 walls were collected in a database.

The number of storeys varies from five to thirteen—corresponding to a total building height ranging from 12 to 33 m—with an interstorey height of around 2.4–2.5 m. The typical thickness of the walls, which is not always constant within the same building, varies between 80 and 150 mm (Fig. 1a). The length of the walls is also variable (from 0.5 to 6.5 m) with an average length of 2 m. The wall web is in general reinforced with a welded mesh with a bar diameter of 5.5–8 mm. This mesh is extended to the wall end regions, and in some cases no further reinforcement is placed. In other cases, longitudinal rebars are added to the boundary elements, whose length is about 10–35% of the entire wall length and have an average reinforcement ratio of 2% (Fig. 1b). In almost 90% of the webs the reinforcement is placed in a single layer; for boundary elements this percentage reduces to approximately 60% since it is not uncommon to add a second layer only in the end regions of the wall. The minimum wall thickness for which a second layer of reinforcement is added in the boundary elements is 120 mm; the wall thickness is typically constant along the wall length. When a single layer is used, the bar diameters in the boundary element never exceeds 25 mm (#8). This layer is often not placed at the centre of the wall but with a certain eccentricity with respect to the wall axis. Eccentricities up to 20 mm were computed from the reviewed construction drawings (Fig. 1c). Additional variability on the rebar position is unavoidable in construction practice due to the use of spacers that can slightly move or rotate during the casting.

The properties of the construction materials vary widely. The typical concrete strength in Colombian construction is between 21 and 35 MPa (Mejia et al. 2004), but lower values are also obtained (Carrillo et al. 2013). With regard to the reinforcement, the minimum
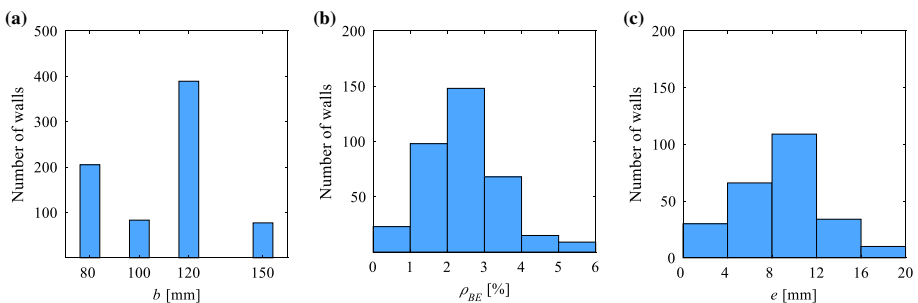


**Fig. 1** Frequency distribution of walls in nine buildings in the city of Cali, Colombia, with respect to the following variables: **a** thickness; **b** reinforcement content in the boundary elements (when present); **c** eccentricity of the longitudinal reinforcement with respect to the cross-section axis

strength values prescribed by the Colombian standard (NSR-10 2010) are 420 MPa for the yield strength ($f_y$), 550 MPa for the ultimate strength ($f_u$), and 1.25 for the ratio $f_u/f_y$. The characteristic values obtained for the reinforcement usually employed in construction practice tend to be slightly higher ($f_y = 470$ MPa, $f_u = 660$ MPa, González et al. 2005).

## 2.2 Test unit design

Based on the discussion in the previous section, the test units were designed to have a single layer of longitudinal reinforcement and the following variable parameters: (1) thickness; (2) reinforcement content and/or bar diameter; (3) eccentricity of the reinforcement with respect to the section centreline. Although 120 mm is the mode of the thickness distribution, specimens from 80 to 100 mm were tested due to the anticipated larger susceptibility to out-of-plane instability. Four different reinforcement contents were investigated, from 0.28 to 3.8%, while bar diameters were varied between 6 and 22 mm. Finally, two eccentricities were considered, 8 and 24 mm, which represent a standard and an upper-limit value.

The specimens were 300 mm long (see Fig. 2b), which corresponds to a lower-bound of commonly employed boundary element lengths in walls. This same length was also considered in the design of the prototype wall units TW1 and TW4, previously tested by the authors (Almeida et al. 2016). It is shown later that the assumed length was sufficient to induce out-of-plane instability in the direction of the thickness, as intended, while minimizing test unit construction costs. The longitudinal reinforcement was placed in a single eccentric layer. The horizontal reinforcement consisted of 16 bars of diameter 6 mm
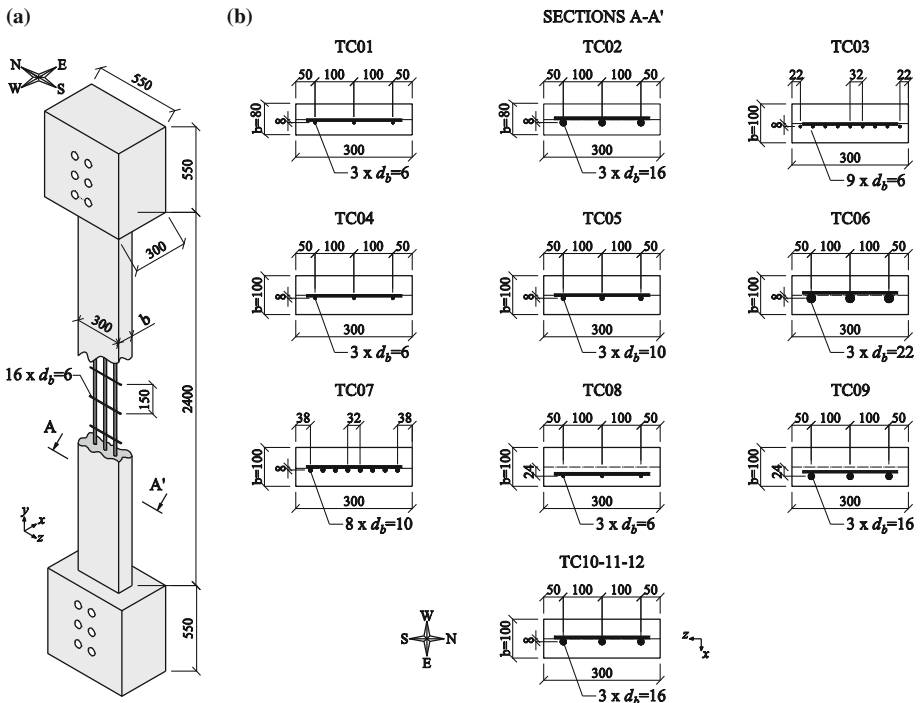


Fig. 2 a 3D sketch of specimens TC10–11–12; b cross-section of all tested specimens (dimensions in mm)

placed at a distance of 150 mm. The foundation and head were stiff RC blocks. The height of the test units ($h_{tot} = 2.4$ m, see Fig. 2a) was chosen to correspond to the typical interstorey height. This choice was supported by recent experimental results from the two thin RC walls aforementioned, suggesting that the entire storey height is involved in the out-of-plane mechanism (Rosso et al. 2016). It is important to note that the imposed boundary conditions of the test setup, which are further discussed in the following section, do not allow to reproduce the complex strain gradient profile occurring in RC walls. This simplification, which existing phenomenological models also assume (Paulay and Priestley 1993), hinders the direct extrapolation of findings to RC wall behaviour. This is of course a rather strong simplification, which make the results herein obtained only directly applicable to walls with very large shear span to storey height ratios. In order to understand the effects of these differences and address this gap, advanced numerical simulations and an improved equivalent boundary element model was recently developed by the authors (Rosso et al. 2017b).

In total, 12 boundary elements were tested. The characteristics of each thin column 'TC' are shown in Table 1 and Fig. 2b. Specimens TC10, TC11 and TC12 had identical properties and are herein considered as the reference test units: 100 mm thick, longitudinal reinforcement composed of three 16 mm diameter bars (i.e., reinforcement ratio of $\rho_{BE} = 2.01\%$) at an eccentricity of 8 mm. The other specimens were tested in order to study the influence of the following parameters: (1) thickness: TC01 and TC02 were thinner than the reference specimens (80 mm); (2) longitudinal reinforcement content: it was varied, in TC03 through TC06, from 0.28 to 3.80%; both the diameter and the number of bars were changed, with the intention of investigating separately each of these parameters; (3) eccentricity: the longitudinal rebars in TC08 and TC09 were placed at a larger eccentricity of 24 mm. Table 1 also shows the line style that will be used for the plots in Sect. 4: the colour for the reference units is blue and triangular-shaped markers.

**Table 1** Description of the test specimens

| Test units | $l$ (mm) | $h_{tot}$ (mm) | $b$ (mm) | $\rho_{BE}$ (mm) | $d_b$ (mm) | No. bars | $e$ (mm) | Line style |
|---|---|---|---|---|---|---|---|---|
| TC01 | 300 | 2400 | 80 | 0.35 | 6 | 3 | 8 | |
| TC02 | 300 | 2400 | 80 | 2.51 | 16 | 3 | 8 | |
| TC03 | 300 | 2400 | 100 | 0.85 | 6 | 9 | 8 | |
| TC04 | 300 | 2400 | 100 | 0.28 | 6 | 3 | 8 | |
| TC05 | 300 | 2400 | 100 | 0.79 | 10 | 3 | 8 | |
| TC06 | 300 | 2400 | 100 | 3.80 | 22 | 3 | 8 | |
| TC07 | 300 | 2400 | 100 | 2.09 | 10 | 8 | 8 | |
| TC08 | 300 | 2400 | 100 | 0.28 | 6 | 3 | 24 | |
| TC09 | 300 | 2400 | 100 | 2.01 | 16 | 3 | 24 | |
| TC10 | 300 | 2400 | 100 | 2.01 | 16 | 3 | 8 | |
| TC11 | 300 | 2400 | 100 | 2.01 | 16 | 3 | 8 | |
| TC12 | 300 | 2400 | 100 | 2.01 | 16 | 3 | 8 | |

$l$ length; $h_{tot}$ height; $b$ thickness; $\rho_{BE}$ longitudinal reinforcement content; $d_b$ diameter of the bars; *No. bars* number of bars used; $e$ eccentricity of the longitudinal reinforcement with respect to the section centreline
*Line style* used in the plots

Walls with a smaller thickness (80 mm instead of 100 mm) are assigned a green marker. Walls with a larger eccentricity (24 mm instead of 8 mm) are indicated by a red marker. Different markers are used to distinguish between the different bar diameters, and they are filled when more than three rebars are used.

The specimens were casted horizontally, three at a time. In order to ensure accuracy in the placement of the reinforcement, special spacers, whose height depended on target eccentricity and bar diameter, were used to support the longitudinal reinforcement inside the formwork. The concrete characteristics are summarized in Table 2 and the reinforcement properties are summarised in Table 3. Unfortunately, the diameter 10 mm bars did not comply with the steel class requested to the steel-provider (CEN 2004), instead a-posteriori tests showed that their ultimate tensile strain was smaller than 5% and the ratio between ultimate and yield strengths was just 1.07. These features influenced the behaviour of specimens TC05 and TC07, as discussed later.

## 2.3 Test setup and loading protocol

The test setup used in this experimental program is shown in Fig. 3a. The top and bottom RC blocks of each specimen were clamped between T-shaped steel profiles, which in turn were connected to the plates of a press. This configuration was intended to be representative of fixed–fixed boundary conditions. The displacement is imposed by the piston at the machine base, which has a stroke of $\pm 125$ mm and a force capacity of $+2.5$ MN in tension and $-10$ MN in compression.

The test was performed in deformation control, where the vertical displacement was averaged from the measurements provided by four vertical LVDTs gaging the elongation between the top and bottom block (Fig. 3a, b). The LVDTs were placed at the corners of the bottom block, and connected to the top block through a plumb line system. The three-dimensional displacement fields of the two shorter sides of the specimens (i.e., North and South faces, see Fig. 2a, b) were recorded using an optical triangulation measurement system and 186 infrared light emitting diodes (LEDs) that were glued to the surfaces of the test units. They were placed on a regular grid of 40 mm along the horizontal direction (or 30 mm for the specimens with reduced thickness) by 100 mm along the vertical direction (totalling 150 markers distributed over 25 rows and 3 columns per side, see Fig. 3a). The remaining 36 LEDs were placed on the top and bottom blocks and on the steel profiles of the test setup. The employed hardware, involving two cameras with three digital optical sensors each (one camera is visible in Fig. 3a), as well as the software, are part of the

**Table 2** Summary of results from concrete compression tests and double-punch tests

| Test units | TC01, TC02, TC08 | TC03, TC05, TC07 | TC04, TC06, TC09 | TC10, TC11[a] | TC12[a] |
|---|---|---|---|---|---|
| $f_c$ (MPa) | 23.7 | 25.7 | 32.3 | 32.9 | 33.6 |
| $E_c$ (GPa)[b] | – | – | – | 29.7 | 28.9 |

$f_c$ Compression concrete cylinder strength, determined from 3 tests per test unit according to SIA (1989). $E_c$ modulus of elasticity determined from specific compression tests

[a]Although specimens TC10, TC11 and TC12 were cast together, the concrete had a slightly different amount of water and therefore separate compressive tests were performed for each specimen

[b]The Young modulus derivation (according to SIA 1989) was performed only for the first three specimens tested (reference specimens)

**Table 3** Summary of results from rebar tensile tests

| Test units | TC01, TC03, TC04, TC08 | TC05, TC07 | TC02, TC09, TC10, TC11, TC12 | TC06 |
|---|---|---|---|---|
| $d_b$ (mm) | 6[a,b] | 10[a] | 16 | 22 |
| $f_{s,y}$ (MPa) | 475 | 545 | 526 | 566 |
| $f_{s,u}$ (MPa) | 625 | 582 | 617 | 663 |
| $f_{s,u}/f_{s,y}$ (−) | 1.32 | 1.07 | 1.17 | 1.17 |
| $\varepsilon_{s,u}$ (%) | 9.8 | 3.7 | 10.3 | 8.7 |
| $E_s$ (GPa) | 184 | 200 | 216 | 199 |

$d_b$ diameter of the bars; $f_{s,y}$ yield strength; $f_{s,u}$ ultimate tensile strength; $\varepsilon_{s,u}$ ultimate tensile strain; $E_s$ modulus of elasticity

[a]This steel does not have yield plateau

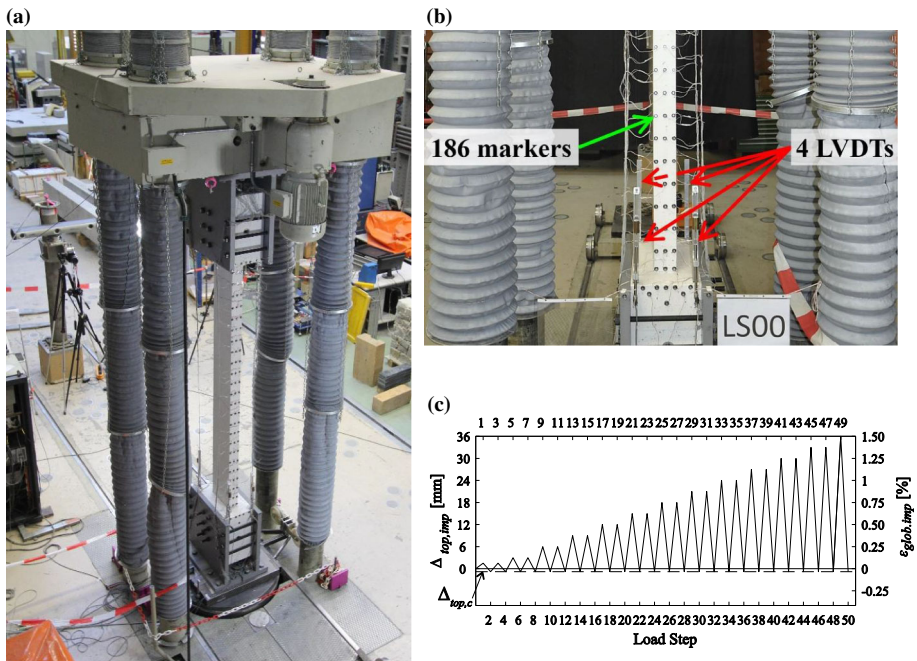[b]This steel was used also for the horizontal reinforcement of all specimens



**Fig. 3** **a** Overview of the test setup; **b** close-up of the measurement systems; **c** loading protocol applied to the specimens ($\Delta_{top,imp}$ is the displacement imposed at the top, while $\varepsilon_{glob,imp} = \Delta_{top,imp}/h_{tot}$). Note that $\Delta_{top,c} = (0.3 \cdot f_c \cdot h_{tot})/E_c)$

commercial system NDI Optotrak Certus HD (NDI 2009). The specimens were always placed in the testing machine with the eccentric longitudinal reinforcement located towards East (cf. cardinal points and reference system in Fig. 2).

The loading protocol consisted of quasi-static cyclic tension–compression axial displacements applied as described next. The peak displacement in the negative (compressive) direction was kept the same in every cycle ($\Delta_{top,c}$). It was computed to correspond to an

average compressive stress of $0.3 \cdot f_c$, assuming that the concrete behaves elastically in this range (i.e., $\Delta_{top,c} = (0.3 \cdot f_c \cdot h_{tot})/E_c$); therefore, a constant displacement between $-0.6$ and $-0.8$ mm (depending on the concrete strength of each specimen) was imposed in the cycles in compression. The peak displacements in the positive (tensile) direction were applied as follows: 1.5 mm → 3 mm → 6 mm, after which the peak displacements were increased incrementally by 3 mm up to failure. This increment was selected because the calculated yield displacement for all the test units is approximately 6 mm. Two cycles were imposed at each amplitude of tensile displacement. The peak values of the imposed displacements are herein denoted by LS, which stands for 'load step'. The imposed displacement history up to a tensile displacement of 36 mm is depicted in Fig. 3c. Only during the tests of specimen TC12 the applied loading protocol was slightly different, as it will be discussed in Sect. 3.1.

# 3 Description of the test results

## 3.1 Description of the behaviour of the test units

In the following, the behaviour of each specimen is briefly presented. Figure 4 plots the axial force–displacement ($F$-$\Delta_{top}$) responses of all tests. They mostly display a stable hysteretic behaviour with appreciable dissipation of energy in tension. After reaching the peak tensile displacement in each cycle, a small drop in the force can be observed: this is related to the fact that, after each load step, the test was temporarily halted in order to take pictures and collect information on the crack development; this break allowed not only for a small reduction in the pump pressure of the testing machine, but also for rebar and concrete stress relaxation. Figure 5 plots the out-of-plane displacement ($\Delta_{oop}$) at the height where the maximum out-of-plane displacement developed ($h$) versus the vertical displacement at the top (the global strains depicted on the right ordinate axis are calculated as the vertical displacement divided by the total height of the test unit, i.e., $\varepsilon_{glob} = \Delta_{top}/h_{tot}$). In the descriptions of the test results, it is assumed that significant out-of-plane deformations are those occurring for lateral displacements equal to or larger than 10% of the specimen thickness.

*TC01* Test units TC01 and TC02 were designed to study the influence of a smaller thickness on the out-of-plane response. In specimen TC01, after the application of the first tensile displacement (LS01), a few cracks opened along the height of the specimen. New cracks appeared during the following cycles up to an applied vertical displacement of 12 mm (LS17, equivalent to a tensile global strain of 0.5%), with an average spacing of about 250 mm. For larger values of vertical displacement only an increase of the crack width was observed. The first significant out-of-plane deformations occurred towards West (LS17–LS18), attaining a maximum out-of-plane displacement of $-18.7$ mm. During the second cycle at the same vertical displacement (LS19–LS20), the specimen displaced to the opposite side (i.e., towards East), attaining a maximum out-of-plane displacement of 18.1 mm. In the following cycles the lateral deformation continued to occur towards East, attaining a maximum out-of-plane displacement of 56.3 mm at 1100 mm above the base ($0.46 h_{tot}$) between LS27 and LS28 (corresponding to $0.704 b$, see Fig. 6a). In the following cycle (LS29), at 21 mm of vertical displacement, the crack pattern of the North–South sides was very symmetric, the maximum crack width was $\sim 4$ mm at around 1120 mm above the base. While loading in compression (LS29–LS30) significant out-of-plane
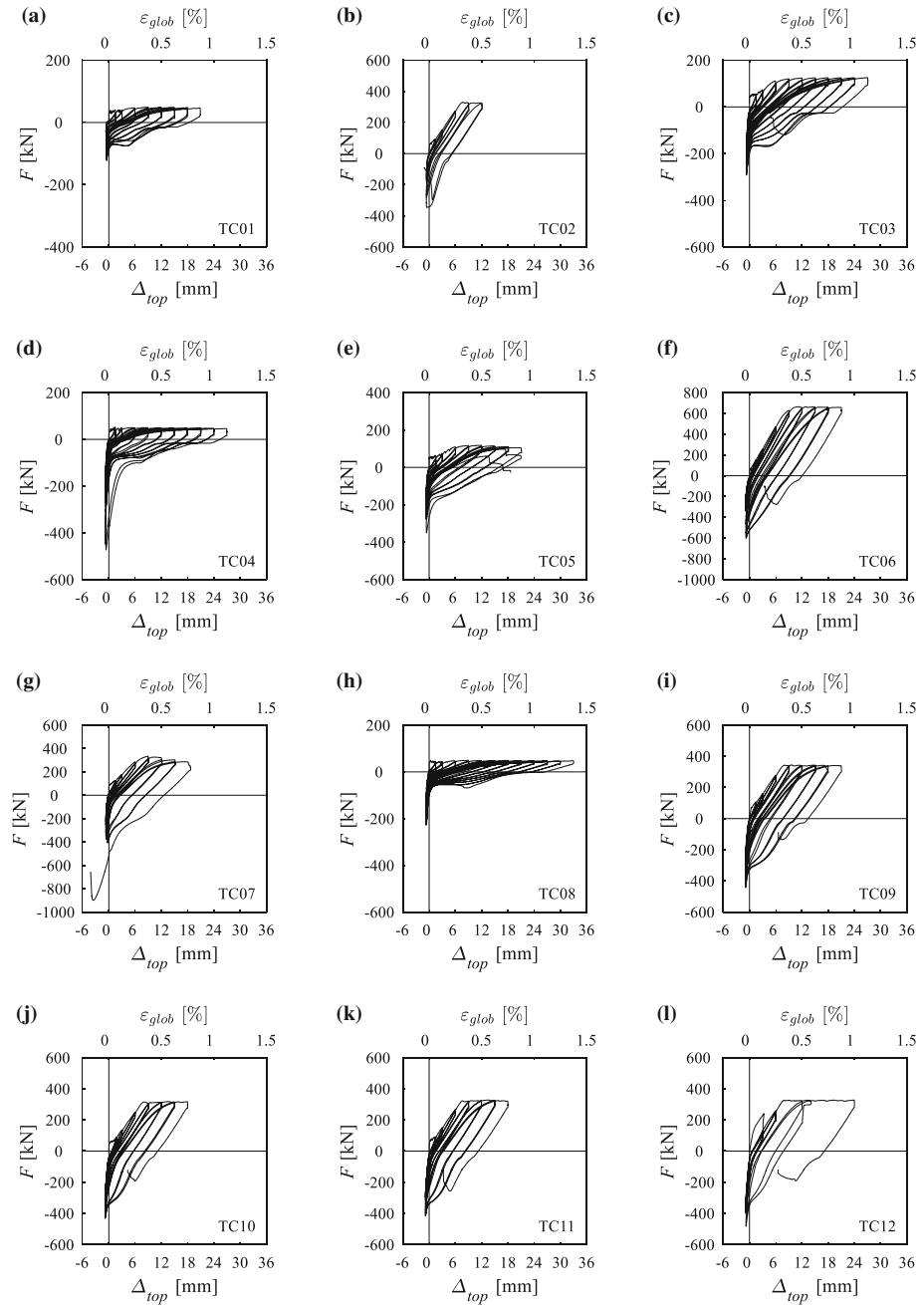
**Fig. 4** Vertical force (*F*) versus vertical displacement (Δ_*top*) responses for specimen (ε_*glob* = Δ_*top*/h_*tot*): **a** TC01; **b** TC02; **c** TC03; **d** TC04; **e** TC05; **f** TC06; **g** TC07; **h** TC08; **i** TC09; **j** TC10; **k** TC11; **l** TC12
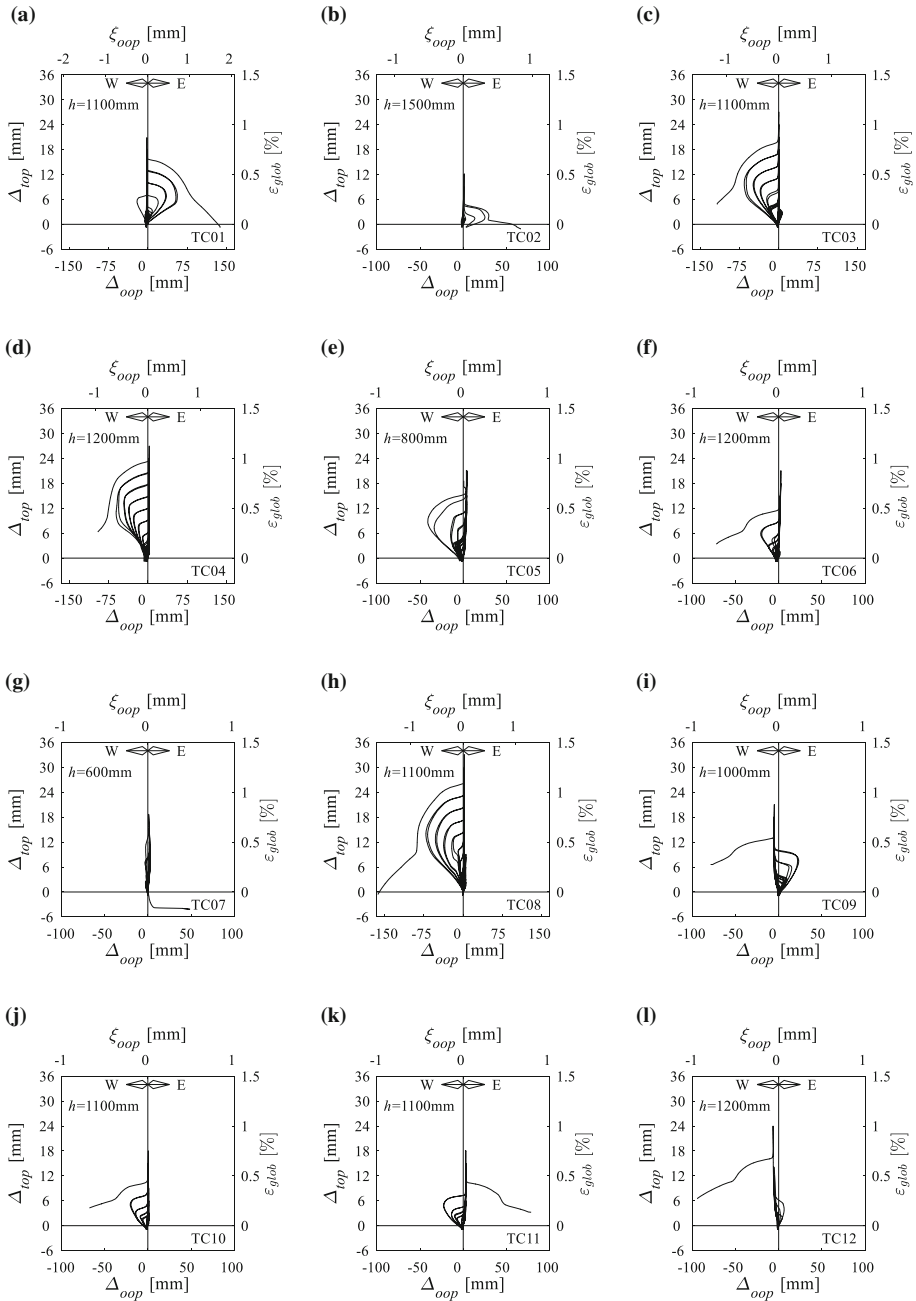
**Fig. 5** Out-of-plane displacement ($\Delta_{oop}$) at the height where it was maximum ($h$) versus vertical displacement ($\Delta_{top}$) for specimen: **a** TC01; **b** TC02; **c** TC03; **d** TC04; **e** TC05; **f** TC06; **g** TC07; **h** TC08; **i** TC09; **j** TC10; **k** TC11; **l** TC12. It is recalled that $\xi_{oop} = \Delta_{oop}/b$ and $\varepsilon_{glob} = \Delta_{top}/h_{tot}$
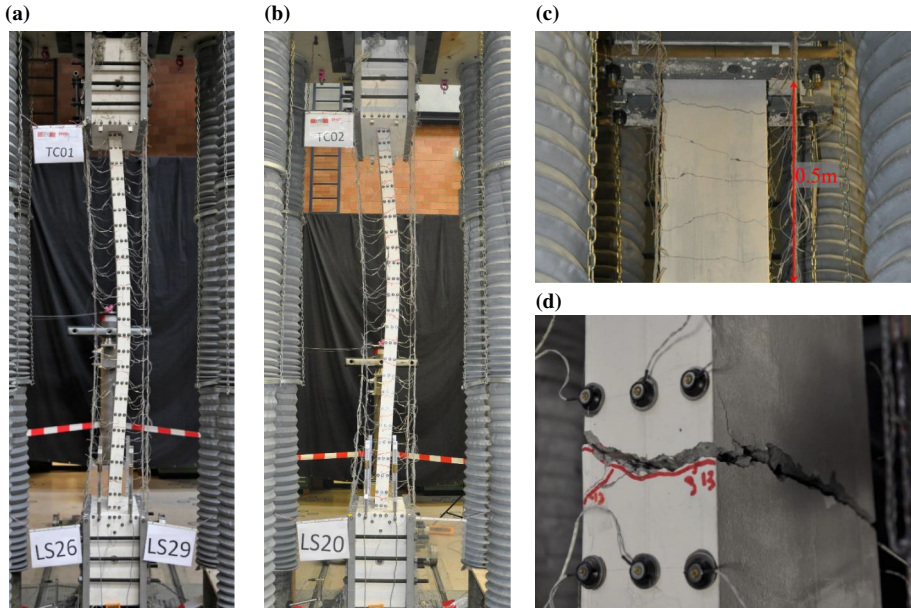
**Fig. 6** **a** TC01 at maximum out-of-plane displacement recovered; **b** TC02 at out-of-plane failure; **c** TC03: detail of the crack spacing on the East side at LS37; **d** TC04: detail of the crack located 1650 mm above the foundation at LS37

deformations took place and, at a lateral displacement of around 67 mm concrete crushing occurred on the West face and the out-of-plane displacements could not be recovered; this marked the failure of the test unit and the test was stopped shortly after. Visual inspection of the specimen after failure identified three hinges: one at the base and a middle hinge at about 1120 mm above the base.

*TC02* At the end of the first load step several thin cracks were visible along the height, spaced on average at around 120 mm. At 12 mm of vertical displacement (LS17, equivalent to a global tensile strain of 0.5%) spalling started to occur in the base and top cracks. The maximum crack width was around 2 mm at midheight, in two cracks located 1200 and 1520 mm above the base. While loading in compression (LS17–LS18), the specimen attained an out-plane-displacement of 25.7 mm towards East at 1400 mm above the base ($0.58h_{tot}$). During this cycle, the test unit almost reached out-of-plane failure since crushing in the plastic hinge at midheight seemed about to commence; this observation was confirmed during the specimen inspection at LS18, where thin vertical cracks above and below the cracks at midheight were detected on the compression side, signalling the onset of concrete crushing. During the second cycle at the same strain level (LS19–LS20), the test unit attained a slightly larger out-of-plane displacement of 27.5 mm, which triggered concrete crushing also in the cracks at the specimen ends, leading to out-of-plane failure and to the conclusion of the test. Although the out-of-plane displacement profile initially resembled a four-hinge mechanism (with hinges at the base, top, and at heights of 1200 and 1520 mm, corresponding to 0.5 and $0.63h_{tot}$), after failure the deformed shape was closer to a three-hinge one, with the middle hinge located 1520 mm above the base (see Fig. 6b).

*TC03* Test unit TC03 (as well as TC07) was designed to study the influence of the reinforcement content. Further, it had roughly the same reinforcement ratio as specimen

TC05 but smaller bar diameter, which also allowed investigating the influence of this latter parameter. Specimen TC03 had the largest number of rebars within the section. In order to assure a sufficient anchorage length to the longitudinal reinforcement in the rigid concrete blocks, four bars out of nine were bent just after the end of the test unit (since the presence of the holes used to apply the usual prestress to the blocks did not allow a deeper anchorage). A similar poor detailing choice caused an undesirable behaviour in specimen TC07, which was tested before TC03. Therefore, the concrete blocks of specimen TC03 were also prestressed along the vertical direction to avoid the appearance of cracks, which could potentially affect the response. This additional prestressing system implied some minor adjustments on the position of the four LVDTs and of some LED markers. This precaution allowed to run the tests normally, without any local damage to the blocks.

During the first excursion into tension several cracks developed showing an average spacing of around 200 mm. At 6 mm of vertical displacement (LS09, equivalent to a tensile strain of 0.25%), vertical splitting cracks appeared on the short sides, aligned with the position of the longitudinal reinforcement. The appearance of these cracks is related to the smaller cover concrete of the longitudinal reinforcement in comparison to the other specimens. The first significant out-of-plane deformation appeared in the first cycle at 15 mm (equivalent to a tensile strain of 0.625%, between LS21 and LS22) towards West, while the maximum out-of-plane recovered was $-66.6$ mm at a height of 1200 mm ($0.5h_{tot}$) during the second cycle at 1% tensile strain (LS35–LS36). At a vertical displacement of 27 mm (LS37, equivalent to a tensile strain of 1.125%) the specimen showed well distributed cracking along the height, with an average crack spacing of 100 mm (see Fig. 6c). While loading in compression to LS38, extensive crushing occurred almost at midheight on the East intrados side. After failure, three hinges were visually identified in the deformed out-of-plane profile: at the base, at midheight, and at around 100 mm below the top block.

*TC04* In specimen TC04, after having applied 1.5 mm of vertical displacement (LS01, equivalent to a tensile strain of 0.0625%), only three cracks appeared along the height: at around 130, 1200 and 2190 mm above the foundation (corresponding to 0.05, 0.5 and $0.91h_{tot}$). At a vertical displacement of 3 mm (LS05, equivalent to a tensile strain of 0.125%) other two cracks formed at around 700 and 1650 mm above the base (0.29 and $0.69h_{tot}$). After this stage no other cracks developed, and only these five would reopen further, up to the failure of the test unit. The first significant out-of-plane occurred towards West during the first cycle at 0.5% tensile amplitude, and in the following load steps they increased up to $-60.5$ mm, which was recovered in the second cycle at 1% tensile strain (recorded at 1200 mm, $0.5h_{tot}$, above the foundation). At 27 mm of vertical displacement (LS37, equivalent to a tensile strain of 1.125%) the crack width varied from 3 to 11 mm; the largest crack was the one located at 1650 mm above the foundation. At this load step, offsets in the cracks along the thickness were also visible even with the naked eye (see Fig. 6d). The failed configuration approached a four-hinge mechanism (excluding the crack at 700 mm), wherein the majority of the crushing was concentrated at midheight and in the top part (see Fig. 7a).

*TC05* Following the application of the first loading cycles, the cracks were well distributed along the element height, at an average spacing of 250–300 mm. At 12 mm of vertical displacement (LS17, equivalent to a tensile strain of 0.5%), the two cracks between the specimen and the concrete blocks were clearly wider than the cracks along the height ($\sim 3$ versus 1 mm, see Fig. 7b), and spalling initiated in the crack close to the head. The crack concentration at the extremities can be related to: (1) the geometrical discontinuity between the concrete blocks and the test unit, which favoured the appearance of quasi-
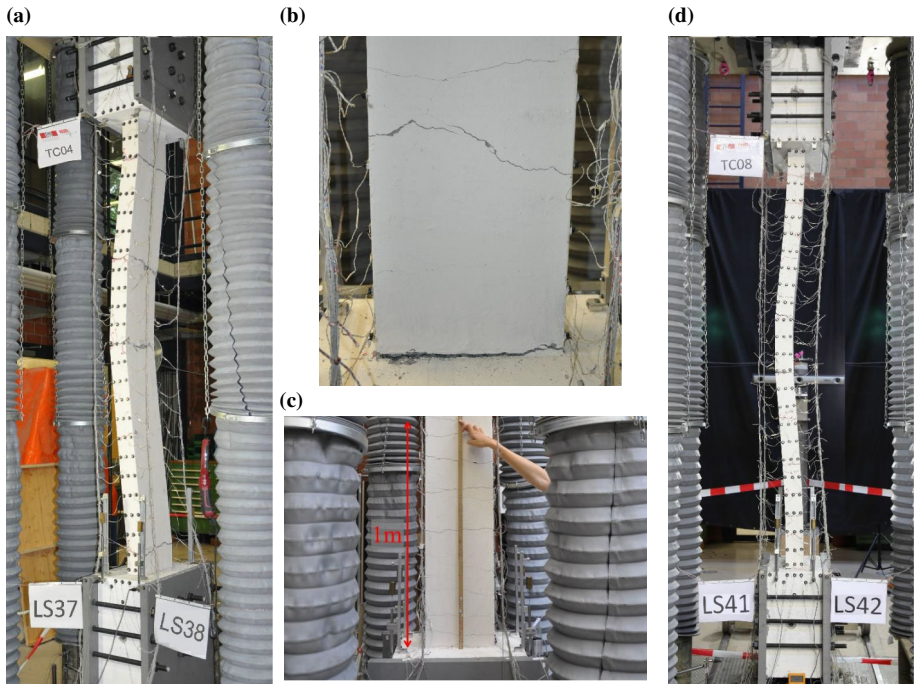
Fig. 7 **a** TC04 at out-of-plane failure; **b** TC05: detail of the crack pattern on the West side in the *bottom part* of the specimen at LS17; **c** TC06: detail of the crack spacing on the East side at LS29; **d** TC08 at maximum out-of-plane displacement recovered

horizontal cracks at the ends (applies to all specimens); (2) the close-to-unity ratio $f_u/f_y$ of the low-ductility steel used in this specimen, which led to large crack spacing. Due to this concentration of damage at the ends, during the second cycle at 0.875% tensile strain amplitude (while loading to LS31) one bar fractured in the base crack. Reloading back to compression (to LS32), an out-of-plane displacement of −41 mm at a height of 800 mm ($0.33h_{tot}$) was attained and recovered. At this stage, an initial onset of crushing was observed in the East-South corner of the specimen, leading to believe that the previous out-of-plane displacement could be close to the critical irrecoverable one. Finally, during the application of a tensile displacement to 24 mm (i.e., to LS33) the other two longitudinal rebars fractured at the base, driving the end of the test. Although out-of-plane failure was not achieved, based on the previously observed onset of crushing in the second cycle at 0.875% tensile strain, it is herein assumed that the tensile strain leading to out-of-plane failure would have been 1%.

*TC06* TC06 was the specimen with the largest reinforcement content of the experimental program. At the first load step (LS01) several thin cracks had opened along the height. In the following cycles, the number of cracks increased further, reducing the spacing to ∼100 mm (see Fig. 7c). The first significant out-of-plane deformation occurred towards West in the first cycle at 0.75% tensile strain (LS25–LS26), attaining a maximum of −21.9 mm in the second cycle, at 1200 mm ($0.5h_{tot}$) above the foundation. At 21 mm of vertical displacement (LS29, equivalent to a tensile strain of 0.875%) spalling was observed in the crack between the test unit and the top block, the maximum width was 2 mm in the top part while in the bottom part it was around 1.2 mm. When loading in

compression (LS29–LS30), at an out-of-plane displacement of around −35 mm, concrete crushing initiated at the base and at 820 mm above the foundation. The test was stopped shortly after, upon a significant lateral displacement increase. The failure configuration approached a three-hinge mechanism.

*TC07* Specimen TC07 had the same reinforcement ratio of specimens TC10–11–12 but smaller bar diameter. It showed problems similar to the ones described for specimens TC03 and TC05 (poor rebar detailing inside the concrete blocks and low ductility of steel). At 12 mm of vertical displacement (LS17, equivalent to a tensile strain of 0.5%), the base crack was much wider than the others, and several cracks appeared in the concrete blocks. The test was continued up to a tensile displacement of 18 mm (LS25, equivalent to a tensile strain of 0.75%), but the presence of a single wide crack along the test unit height prevented the development of out-of-plane deformations. Therefore, it was decided to load this specimen up to compression failure, which was attained through sudden concrete crushing 700 mm above the foundation.

*TC08* Test units TC08 and TC09 were designed to study the influence of the longitudinal rebar eccentricity with respect to the centreline of the cross-section, which was therefore increased from 8 to 24 mm. During the first tensile cycles, specimen TC08 presented more extensive cracking on the East side whereas only a few cracks were visible on the West surface. The cracks on the East side opened at a spacing approximately equal to the spacing of the horizontal reinforcement (150 mm). At a tensile displacement of 18 mm (LS25, 0.75% average tensile strain), fourteen and eight cracks were counted on the East and West sides respectively. When loading in compression, the first significant out-of-plane deformations (towards West) occurred. The differences in the crack pattern between the two sides were lessened during the following cycles. At 30 mm of vertical displacement (LS41, equivalent to a tensile strain of 1.25%), they were roughly symmetric. The largest crack width (of about 10 mm) occurred in the crack between test unit and the head block. During the second cycle at 1.25% tensile strain, an out-of-plane displacement of −72.2 mm (corresponding to $0.722b$, see Fig. 7d) towards West was attained and recovered, 1400 mm ($0.58h_{tot}$) above the foundation; this was the largest out-of-plane displacement recovered during the entire experimental program. During the next cycle, from 1.375% tensile strain while loading in compression (LS45–LS46), out-of-plane failure occurred. The deformed shape after failure mechanism seemed to consist of three plastic hinges, with extensive crushing occurring almost at midheight.

*TC09* Specimen TC09 was mistakenly placed in the testing machine in mirrored position with respect to the other test units (i.e., the longitudinal reinforcement eccentricity was towards the West instead of East). However, during the post-processing of the measurements, the data was corrected to be consistent with the other specimens, and therefore in the following the reference system (and cardinal points) shown in Fig. 2 are used, similar to the remaining units, instead of the original one during the testing. At the first load step (LS01), TC09 developed several thin cracks on the East side (maximum width of 0.1 mm), while on the West side only four wider cracks formed (maximum width of 0.5 mm). This asymmetry in the crack pattern was completely overcome at 9 mm of applied vertical displacement (LS13, equivalent to a tensile strain of 0.375%), and the largest crack was located 980 mm above the foundation. The first significant out-of-plane deformation occurred towards East in the first cycle at 0.65% tensile strain. The largest out-of-plane displacement recovered of 23.2 mm was attained towards East, 1000 mm ($0.42h_{tot}$) above the foundation, in the second cycle at 0.75% tensile strain. While loading in compression after a tensile displacement of 21 mm (LS29–LS30), a large out-of-plane deformation towards the opposite side (West) occurred, the out-of-plane displacement

increased rather quickly causing extensive crushing at midheight, and the test was stopped soon after. Also for this specimen the deformed out-of-plane profile after failure resembled a three-hinge mechanism.

*TC10* After the application of the first tensile displacement, several cracks developed along the height, roughly at a spacing equal to the horizontal reinforcement spacing (150 mm). The first significant out-of-plane displacement occurred towards West while loading in compression after a tensile displacement of 12 mm (LS17, equivalent to a tensile strain of 0.5%). In the second cycle at 15 mm (i.e., 0.625% tensile strain), an out-of-plane of −20.7 mm towards West was attained at 1100 mm ($0.46h_{tot}$) above the base and then recovered upon further compression. At a vertical displacement of 18 mm (LS25, equivalent to a tensile strain of 0.75%), the largest cracks were concentrated above the base of the test unit, with a width of around 1.5–2 mm. While loading back into compression (to LS26), the test was stopped after a large irrecoverable out-of-plane displacement at midheight was attained. From visual inspection, three hinges were identified in the deformed shape after failure.

*TC11* Specimen TC11 was geometrically and mechanically identical to TC10 and it was tested under the same loading protocol in order to investigate the reproducibility of experimental results. The responses of TC11 and TC10 were very similar, although specimen TC11 failed differently. The first significant out-of-plane displacement was observed occurring towards West while loading in compression after a tensile displacement of 12 mm (LS17, equivalent to a tensile strain of 0.5%), and, consistently with unit TC10, the largest lateral displacement recovered (−25.2 mm at 1400 mm above the foundation) was attained in the second cycle at 0.625% tensile strain. At 18 mm of vertical displacement (LS25, equivalent to a tensile strain of 0.75%), four main cracks could be observed: at the base, at 1080 mm, at 1420 mm above the foundation (0.45 and $0.59h_{tot}$,), and at the test unit top. While loading in compression (to LS26), a large out-of-plane deformation towards East occurred, crushing occurred at the ends and in several cracks at midheight, and the test was stopped. Therefore, specimen TC11 failed out-of-plane to the opposite side with respect to the one towards which it had displaced in the cycles before, similarly to TC09. The deformed out-of-plane profile after failure resembled a four-hinge mechanism.

*TC12* Specimen TC12 was also geometrically and mechanically identical to TC10 and TC11. Chronologically, it was the first unit of the experimental program to be tested. Due to a problem with the system controlling the servo-hydraulic actuator, the first tensile displacement applied was 3 mm instead of the planned 1.5 mm. Additionally, in the initially-planned loading protocol the displacement increments between the cycles were larger: namely, the cycles at an amplitude of 9, 15 and 18 mm had been omitted. During the cycles at 12 mm the out-of-plane deformation was small, therefore a tensile displacement of 24 mm (equivalent to a tensile strain of 1%) was applied next. At this load step, large cracks were spread along the height. When the loading was reversed and the specimen loaded in compression, a very large out-of-plane deformation towards West occurred. The out-of-plane displacement attained at midheight had approximately reached −100 mm when loading was stopped. At this point, extensive concrete crushing at midheight and ends was apparent. Four hinges were identified after failure from visual inspection of the out-of-plane profile: one at the base and one at the top, and two almost at midheight at around 1000 and 1400 mm above the base (0.41 and $0.58h_{tot}$). The deformed shape at failure of TC12 was therefore very similar to the one of TC11, although the out-of-plane displacement occurred towards East in the latter case and towards West in the

former unit. Overall, these two specimens showed a mirrored behaviour throughout the tests with respect to the side to which the out-of-plane deformations developed.

## 3.2 Experimental data

The dataset of the experimental program can be downloaded from the publicly accessible platform Zenodo, DOI: 10.5281/zenodo.569799. The structure of the data folders is described in the report 'Data_organization_Rosso_et_al_2017.pdf', also available for download. For each test unit, the following data are provided: (1) Material tests results: results of concrete and rebar tests; (2) Qualitative data: a copy of the laboratory notebook and photos of interesting phases of the test; (3) Unprocessed data: conventional (e.g., LVDTs and load cells) and optical triangulation raw data; (4) Postprocessed data: synchronized and reorganized conventional and optical triangulation data.

# 4 Experimental findings

## 4.1 Global behaviour

*Evolution of the out-of-plane displacements* Several observations can be made with regard to the out-of-plane responses plotted in Fig. 5: (1) Small out-of-plane deformations may occur when the specimens are loaded in tension. This is caused by the asymmetric opening of the cracks due to the rebar eccentricity, inducing a small curvature along the specimen. (2) During the last cycle, the out-of-plane displacement often seems first to stabilize before starting to irrecoverably increase, leading to the out-of-plane failure of the test unit. A similar behaviour was observed by Chai and Elayer (1999) for boundary elements with two layers of reinforcement, associated to the partial closure of the cracks. (3) The principal difference between the tests regards the side towards which each test unit developed out-of-plane deformations. The side did not only differ from specimen to specimen, but also within the same test (e.g., TC01 in Fig. 5a). The only planned source of asymmetry during the tests was the longitudinal rebar eccentricity, whereas unplanned sources of asymmetry include the specimen construction accuracy, material inhomogeneity, minor misalignments of each test unit in the setup, and imperfect rotational restraints at the top and bottom of the element (these rotations were measured during the test). The two specimens in which the
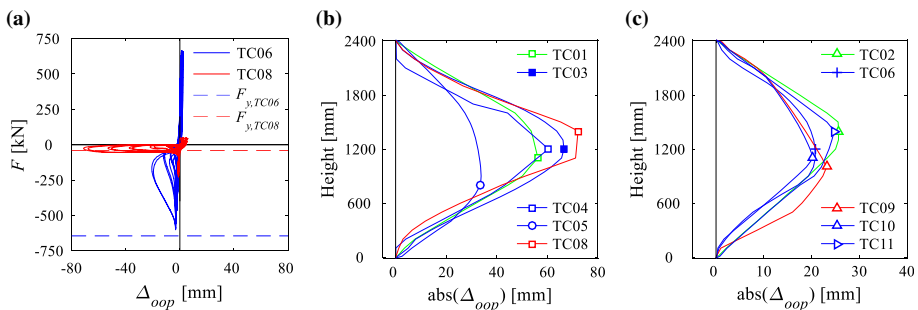


**Fig. 8** **a** Force ($F$) versus out-of-plane displacement ($\Delta_{oop}$) at the height where it was maximum for specimens TC06 and TC08; **b**, **c** Deformed shapes at largest out-of-plane displacement attained and recovered for all specimens (except TC07 and TC12)

rebar eccentricity was largest (TC08 and TC09) buckled towards opposite sides, as depicted in Fig. 5h, i. Therefore, it appears that this parameter alone does not predominantly govern the side towards which the out-of-plane deformation develops.

*Evolution of the compressive forces* Fig. 8a plots for TC06 and TC08 the vertical force versus the out-of-plane displacement at the height where the out-of-plane displacement was maximum. This height in general remained constant once significant out-of-plane deformation started. Specimen TC06, which had the largest reinforcement content, attained the largest tensile and compressive forces, whilst TC08 attained the largest critical tensile strain and recovered the largest out-of-plane displacement. The onset of out-of-plane deformation occurred for small levels of compressive (negative) forces, at values significantly lower than the yield force of the rebars (plotted in Fig. 8a with dashed lines). Therefore, the development of out-of-plane instability in RC boundary elements with a single layer of reinforcement does not imply yielding of rebars in compression, as it will be further discussed in Sect. 4.2. Furthermore, the forces are still lower than the yield force at attainment of maximum out-of-plane displacement, especially in the case of large reinforcement ratios (i.e., TC06). For small reinforcement ratios (i.e., TC08), once the lateral deformation starts the force remains almost constant up to the attainment of the maximum out-of-plane displacement. This observation is also evident from Fig. 4h, in the form of a force plateau in the descending branch from tension to compression. The corresponding shortening of the boundary element is therefore related to the development of significant out-of-plane deformations. This behaviour can be found in almost all specimens, and more distinctly in those developing large out-of-plane deformations. The compressive forces pick up again when the recovery of the out-of-plane deformation starts.

*Deformed shapes at large out-of-plane displacements* Fig. 8b, c plot the deformed shapes at largest recovered out-of-plane displacement for each specimen (except for TC07 and TC12). For the sake of clarity, the figure is divided in two plots, depending on the magnitude of the maximum out-of-plane deformation attained. The heights at which the maximum displacement is attained are identified with a marker. The maxima do not always occur exactly at midheight, but rather at heights between 0.34 and $0.58h_{tot}$ (i.e., between 800 mm and 1400 mm above the base). Specimen TC06 (Fig. 8c) shows the most regular and smooth profile, which can be attributed to a very homogeneous crack distribution along the height. A similar smooth shape can be observed in TC05 (Fig. 8b), wherein—notwithstanding a large crack between the test unit and the foundation—the cracks also spread uniformly. On the contrary, kinks representing plastic hinges can be readily identified for other specimens (e.g., specimen TC04 and TC08).

## 4.2 Local behaviour

### 4.2.1 Local strains and curvatures

From the displacement measurements provided by the optical system, local strains ($\varepsilon_{loc}$) were calculated. Each row was formed by three LEDs—placed along the thickness, 10 mm from the edges and at the centreline of the specimen—at a vertical row spacing of 100 mm, see Sect. 2.3 and Fig. 9a. Three strain values were computed from the vertical displacement variation between each pair of aligned markers in adjoining rows (see circles in Fig. 9b). Subsequently, the 'local strain' profile along the thickness was obtained either from: (1) piece-wise linear interpolation (continuous line in Fig. 9b); this profile is used to derive the strains at the edges and at the rebar location (see '×' marker in Fig. 9b); (2)
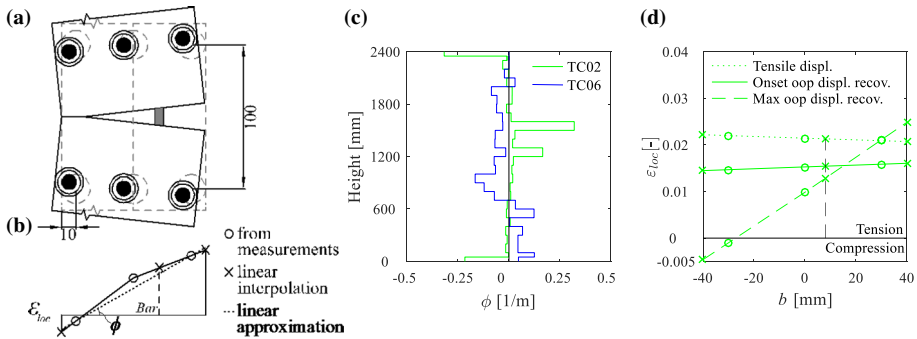
**Fig. 9** **a** Computation of local strains from LED measurements (all dimensions in mm); **b** Curvature profiles along the height of specimens TC02 and TC06, at an out-of-plane displacement of 21.9 mm; **c** Strain profiles along the thickness of TC02 at the height of the plastic hinge at specimen midheight, at maximum tension, and at onset of/maximum out-of-plane (oop) displacement recovered

linear interpolation of the two measurements at the extremities (dotted line named 'linear approximation' in Fig. 9b); this profile is used to calculate the 'local curvatures' ($\phi$).

In the following paragraphs, the behaviour of specimen TC02 is analysed in detail as an example, but the observations are valid for all specimens. As described in Sect. 3.1, TC02 formed four plastic hinges (at $\sim 1200$ and $\sim 1520$ mm from the base, corresponding to 0.50 and $0.63 h_{tot}$ respectively, and at the ends).

*Curvature profile along the total height* The out-of-plane displacement profiles plotted in Fig. 8b-c could suggest a rather smooth curvature profile. However, the experimental results show that the curvatures are not uniformly spread over the height, instead their profile depends strongly on the crack pattern. Figure 9c compares the curvatures along the height between specimens TC02 and TC06 at the same absolute maximum out-of-plane displacement of 21.9 mm (corresponding to the largest value attained by TC06). The value of the local curvature $\phi$ is assumed to be constant between two rows of LEDs. The profile for TC02 has more peaks and, as expected, they concentrate at the heights where the widest cracks form. On the contrary, the profile of TC06 is smoother since the cracks are more uniformly distributed. Therefore, although both test units show smooth out-of-plane displacement profiles, the curvature profiles indicate distinct local rotational demands on the cracks.

*Evolution of the local behaviour* A closer analysis of the local strains yields new insights on how the out-of-plane deformation develops. Figure 9d plots the evolution of the strain profile of the TC02 section at the height of the plastic hinge that formed 1520 mm above the foundation ($0.63 h_{tot}$), during the last cycle for which the out-of-plane deformation was still recovered. Namely, three instants are presented: at maximum tensile displacement applied (dotted line), at the onset of out-of-plane deformation (continuous line), and at maximum out-of-plane displacement (dashed line). When the boundary element is in tension, the strains are obviously positive and the curvature is small. At the onset of out-of-plane displacement, although the member has undergone compressive forces, the strains are all still positive and large, meaning that crack closure has not yet started; the curvature remains small, but of opposite sign with respect to the curvature in tension. At maximum out-of-plane displacement the curvature is significantly larger and compressive strains are visible, indicating crack closure. The fixed supports in the test setup imply that cracks along the height cannot all close on the cross-section side opposite to the rebar
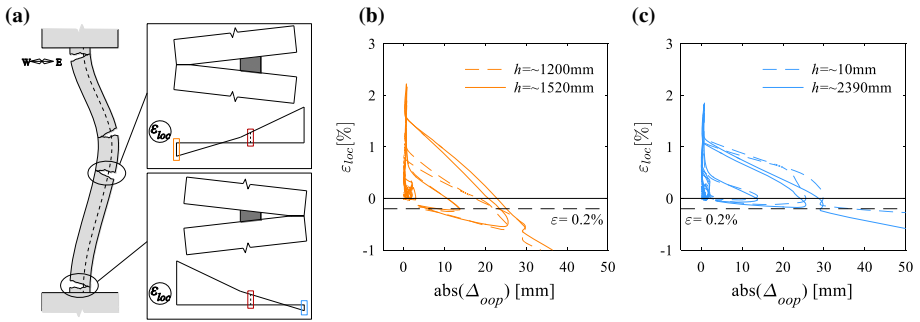
**Fig. 10** TC02: **a** Qualitative sketch of out-of-plane mechanism, including close-ups on crack closure in the four controlling plastic hinges; **b**, **c** Evolution of local strains on the section edge where cracks first closed (West side for cracks at midheight, East side for top and bottom cracks) versus out-of-plane displacement at the height where it was maximum

location. This is illustrated in Fig. 10a, which plots qualitatively the deformed shape of specimen TC02 with particular emphasis on the opening of the four main cracks. If the two cracks at midheight close first on the West side, as illustrated in Fig. 9d, the cracks at the ends have to develop opposite curvatures, closing first on the East side.

*Out-of-plane displacement recovery* After large out-of-plane deformations, crack closure is required on both sides of the section to achieve full recovery. Figure 10a plots qualitatively the strain profiles along the thickness for the cracks at midheight and ends. Figure 10b, c plot the evolution of the local strains on the edge where cracks first closed versus out-of-plane displacement at the height where it was maximum. At maximum tensile displacement, the experimentally derived local vertical strains at the main cracks are significantly larger than the average global tensile strain imposed to the test unit, which is a well-known localization phenomenon (for example, the global tensile strain applied before failure was equivalent to 0.5%, while Fig. 10b, c indicate local tensile strains of approximately 2%). The cracks at midheight close on one side (i.e. reach compressive strains) at smaller values of out-of-plane displacement than cracks at ends: assuming an equal tensile strain at the axis of the reinforcement (this assumption appears to holds well for all hinges at onset of out-of-plane displacement), crack closure occurs at smaller values of curvatures in the hinge at midheight, therefore at smaller values of out-of-plane displacement. The out-of-plane displacement keeps increasing even after the two cracks at midheight attained compressive strains since the cracks at the ends are still open. The closure of the crack at 10 mm above the foundation, in Fig. 10c, can be clearly identified as the reason for out-of-plane displacement recovery. In other words, only crack closure on both sides may trigger a realignment of the specimen.

*Out-of-plane failure criterion based on compressive strain limits* It was observed, from analysis of experimental results, that out-of-plane displacements cannot be recovered when a critical compressive strain value of 0.2% is attained in, at least, three plastic hinges. For the specific case of TC02, in the penultimate cycle (i.e., first cycle at $\Delta_{top} = 12$ mm), the limit compressive strain was exceeded in the two middle hinges (Fig. 10b), but not yet in the ones at the top and bottom (Fig. 10c). In the last cycle (i.e., second cycle at $\Delta_{top} = 12$ mm) this limit strain was also exceeded in the top hinge (at 2390 mm above the base) and therefore out-of-plane failure took place. This was confirmed by visual inspection during testing: when the out-of-plane displacement was recovered, vertical cracks suggesting onset of crushing were observed only in the hinges at 1200 and 1520 mm
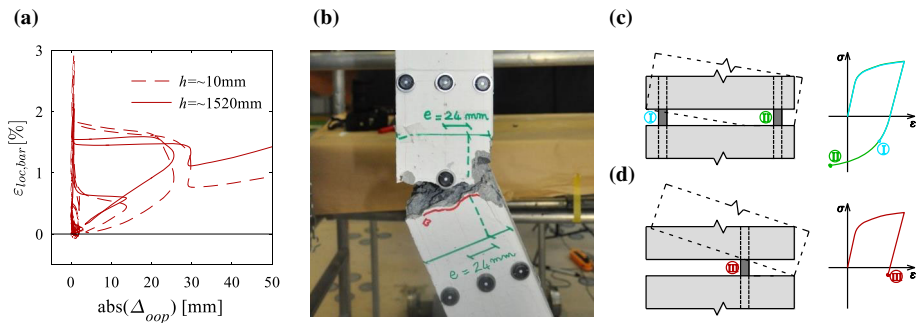
**Fig. 11** **a** TC02: evolution of local strains at the rebar position in two plastic hinges versus out-of-plane displacement at the height where it was maximum; **b** Specimen TC08 after failure; **c**, **d** Description of the onset of out-of-plane instability for members with one or two layers of reinforcement

above the base. Concrete crushing at the unit ends was detected only after failure, when the out-of-plane deformation was no longer recovered. Note that the previous failure criterion does not depend on the base length used to compute the local strains as they refer to the compressive regime before strain-softening localization. This is unlike the tensile regime, where localization tends to show up for low values of strain due to the formation of cracks.

*Rebar acting as sectional rotation pivot point* At the onset of out-of-plane deformation, the reinforcement acts as a hinge around which the regions above and below the crack rotate. Figure 11a depicts the local strains of TC02 at the rebar position (i.e., at an eccentricity of 8 mm from the centreline) as obtained from the interpolation of the measured strains, for the hinge above the foundation and the one 1520 mm above the base. Note that the value of strain does not correspond to the actual strain in the steel rebar but to the average value of strain over the distance corresponding to the spacing between two rows of LEDs. The figure indicates that before the onset of out-of-plane deformation, an elastic strain recovery takes place; the latter was quite variable, taking on values ranging from 0.3 to 1%, but constant in each hinge throughout the test independently of the value of the applied tensile displacement. Following the elastic recovery, the strains remain approximately constant as the out-of-plane displacements increase. Such local strain behaviour differs drastically from the compressive strains at the test unit face, see Fig. 10b, c, suggesting that the single layer of reinforcement in the crack acts as a pivot point. Visual inspection after failure also appears to confirm the above. As an example, Fig. 11b shows a close-up on specimen TC08 at the end of the test, i.e. after attaining irrecoverably large out-of-plane deformations. The position of the reinforcement is highlighted with a green dashed line, and the parts below and above the crack seem to have clearly pivoted around the bar, which thus acted as centre of rotation.

*Out-of-plane instability of single-layered members* The previous finding, together with the observation that the onset of out-of-plane occurs at a much smaller compressive force than the yield force of the rebars (see Fig. 8a; Sect. 4.1), imply that the mechanism of out-of-plane instability in members with one layer of longitudinal reinforcement differs significantly from the mechanism of members with two rebar layers. In the latter case, the reinforcement layer on the compression side needs to yield or buckle in compression before significant out-of-plane displacements can develop (see green line in Fig. 11c). The crack will eventually close on that section edge, while the other rebar has not yet yielded and hence retains a relatively large stiffness (Paulay and Priestley 1993). The development

of the mechanism requires a relatively large compressive force in order to also yield in compression the second layer of reinforcement, and hence the onset of out-of-plane deformations can be expected for large compressive forces. The case of a single-layer boundary elements is distinct: as soon as the member is subjected to a compressive force, the reinforcement in the crack acts like a pivot point around which the member parts above and below can rotate (see Fig. 11d). Therefore, the element can develop large out-of-plane displacements at small values of compressive force.

### 4.2.2 Crack patterns

The crack patterns differed significantly between the test units, and this affected the development of the out-of-plane response and the magnitude of the maximum out-of-plane displacement attained, as discussed next.

*Crack spacing* The average spacing between the cracks was measured qualitatively during the tests, and it was verified a posteriori through the results of the optical measurement system. It is well known that the crack spacing depends on the longitudinal reinforcement content, concrete cover, loading condition (pure tension, pure-bending, or in-between conditions), and on the spacing, diameter and bond properties of the longitudinal rebars (CEB 1978; FIB 2010). Figure 12a compares the average crack spacing in the specimens and reflects the influence of the parameters varied in the experimental program: (1) When the longitudinal reinforcement ratio and the bar diameter decreased, the average crack spacing increased. (2) The eccentricity with respect to the centreline of the section strongly affected the crack spacing in the specimens with small reinforcement content. In fact, comparing specimens which differed only with regard to the reinforcement eccentricity, for a bar diameter $d_b = 6$ mm, the smaller concrete cover caused the occurrence of cracks at a smaller spacing (i.e., TC08 vs. TC04), while for $d_b = 16$ mm the average crack spacing was independent of the bar eccentricity (i.e., TC09 vs. TC10-TC11-TC12).

*Crack width* Crack opening is a function of the crack spacing and the tensile displacement applied. The average crack width for all specimens was calculated using the
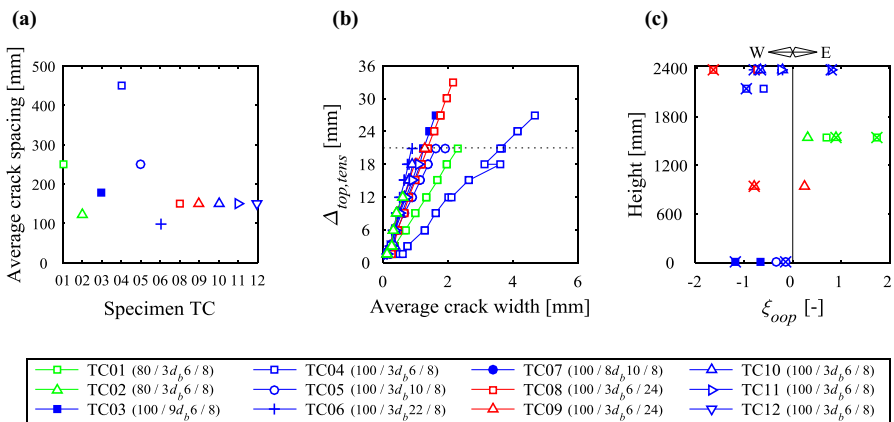


**Fig. 12 a** Average measured crack spacing for each specimen; **b** Average crack width versus applied tensile displacements; **c** Height above the foundation at which the widest crack was located versus normalized out-of-plane displacement ($\xi_{oop} = \Delta_{oop}/b$) in the last two cycles, for all specimens. In legend, in brackets: thickness/reinforcement layout/eccentricity

optical measurements: (1) first, by calculating every two rows the variation in vertical displacement of the three pairs of LEDs, (2) then, by averaging the three values obtained along the row, (3) finally averaging the latter along the total height. The obtained average crack widths are plotted in Fig. 12b versus the tensile displacements applied at the top. Comparing a cycle in which the same tensile displacement was applied, (e.g., 21 mm, see dotted line), the crack width in specimen TC04 was more than two times larger than in specimens TC01 or TC08, which had similar reinforcement content, confirming that the largest average opening was attained in the specimens with larger average crack spacing.

*Influence of the crack pattern on the side to which out-of-plane displacement developed* The side towards which the specimen buckled was unpredictable a priori, however it seemed to depend on the crack distribution over the height. Experimental evidence showed that if the largest crack formed at the ends, the test unit tended to buckle towards the West (i.e., towards the opposite section side of the rebars). Differently, if the largest crack formed in the central part of the specimen, the test unit tended to displace towards East. This finding is shown in Fig. 12c, which plots the height above the foundation at which the widest crack was located versus the maximum normalised out-of-plane displacements ($\xi_{oop} = \Delta_{oop}/b$) attained in the last two cycles of each test. A classical marker represents the largest recoverable out-of-plane displacement attained, while a '×' overlapping the marker signals attainment of out-of-plane failure. As discussed in Sect. 3, some specimens changed buckling side during the test. TC09 and TC11 at failure displaced towards the opposite side compared to the one of the previous cycles, but, as shown in Fig. 12c, the widest crack remained the same throughout the last two cycles. However, a clear increase in opening of other cracks was detected when the largest tensile displacement before failure was applied, and this may at least somehow contribute to justify the change in side. TC01 displaced towards West in the first cycle where significant out-of-plane deformation developed, while it kept buckling towards East in the followings cycles (see Fig. 5a). In this case, an explanation for the change in buckling side was not found, since no clear differences in the crack pattern were identified.
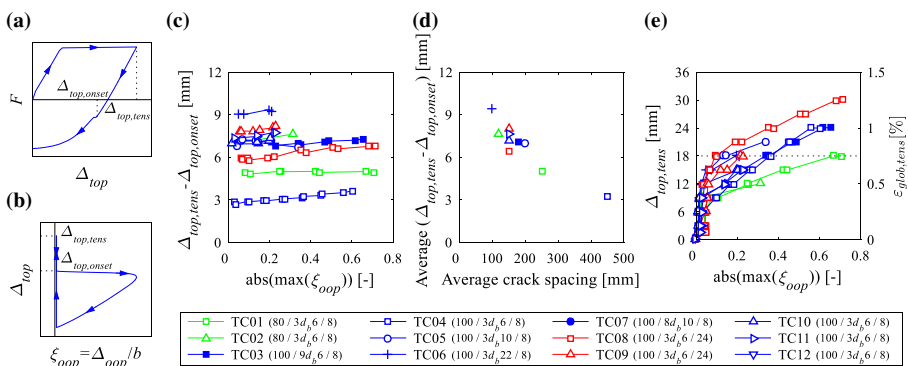


**Fig. 13 a, b** Identification of the vertical tensile displacement imposed at previous load step ($\Delta_{top,tens}$) and of the *vertical* displacement at the onset of out-of-plane deformation ($\Delta_{top,onset}$, corresponding to a lateral displacement $\xi_{oop}$ of 0.01) in the force–displacement and vertical versus out-of-plane displacement curves; **c** difference $\Delta_{top,tens} - \Delta_{top,onset}$ versus absolute normalized out-of-plane displacement at the height where it was maximum; **d** average difference $\Delta_{top,tens} - \Delta_{top,onset}$ versus average crack spacing for each specimen; **e** maximum normalized out-of-plane displacement attained and recovered between two consecutive load steps versus $\Delta_{top,tens}$

*Influence of the crack pattern on the onset of out-of-plane deformation* Fig. 13c plots the difference between the vertical tensile displacement applied at the previous load step ($\Delta_{top,tens}$, see Fig. 13a, b) and the vertical displacement at the onset of out-of-plane deformation ($\Delta_{top,onset}$, corresponding to a lateral displacement $\Delta_{oop}$ of 0.01$b$, see Fig. 13a, b) versus the absolute maximum out-of-plane displacement attained when reloading in compression. It is observed that this difference of vertical displacements, which can be seen as the elastic recovery of the strains in the reinforcement occurring in all the hinges along the member height, remains constant throughout the test. Further, this difference is inversely proportional to the crack spacing as plotted in Fig. 13d.

*Influence of the crack pattern on the maximum out-of-plane displacement attained* Fig. 13e plots the maximum out-of-plane displacement attained and recovered between two consecutive load steps versus the vertical tensile displacement imposed at the previous load step. Focussing on TC01, TC04 and TC08 (which had similar reinforcement content), after applying 18 mm in tension (see dotted line) and reloading in compression, the out-of-plane displacements experienced by each specimen were very different: $\xi_{oop} = 0.671$, 0.357 and 0.092 respectively. The maximum lateral displacement attained can be explained by a combination of the crack width/spacing in tension and the curvature required to attain limit-state values of local strains: wide cracks allow large rotations, and therefore large out-of-plane displacements, but the out-of-plane deformation can be recovered only if the limit compressive strain is not overpassed.

## 4.3 Influence of key parameters investigated

The influence of various parameters on the out-of-plane response is discussed in the following:

*Thickness* Boundary elements with smaller thickness failed at smaller critical tensile strains (see Fig. 14a). In fact, the thickness of specimens TC01 and TC02 was 20% smaller than the thickness of TC04 and TC10–11–12, respectively, and the critical tensile strain was about 22% smaller in TC01 than in TC04 (both reinforced with three rebars $d_b = 6$ mm), and 33% smaller in TC02 than in TC10–11 ($d_b = 16$ mm; note that in TC12 a different loading protocol was applied, see Sect. 3.1).

*Eccentricity* The experimental results seem to point to an unexpected increase in failure-triggering critical tensile strain with an increase in the eccentricity of the
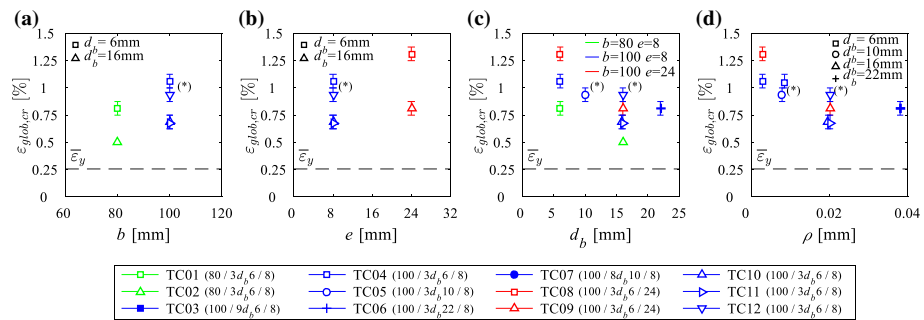


**Fig. 14** Influence on the critical tensile strain of: **a** the thickness; **b** the eccentricity of the longitudinal reinforcement; **c** the bar diameter; **d** the reinforcement ratio. Note that $\overline{\varepsilon_y} = 0.026$ represents the average yielding strain within the experimental program. Asterisks In TC05 failure occurred in tension; in TC12 several cycles were skipped

reinforcement layer (Fig. 14b). The reason is believed to be the crack spacing: the larger the eccentricitiy, the smaller the crack spacing and therefore the larger the failure-triggering critical tensile strain. The difference in critical tensile strain between TC04 and TC08 ($\rho_{BE} = 0.28\%$, eccentricity 8 and 24 mm respectively) was 0.25%, reducing to 0.125% in the case of TC10–11 and TC09 ($\rho_{BE} = 2.01\%$, eccentricity 8 and 24 mm respectively).

*Reinforcement content and bar diameter* A larger reinforcement content in the boundary element led to smaller critical tensile strains causing out-of-plane failure, as plotted in Fig. 14c, d. Specimens TC03 and TC07 were designed with the same reinforcement content of TC05 and TC10–11–12 respectively, but with different rebar diameters in order to separate the influence of the latter parameter from the reinforcement content. Unfortunately, as previously reported, the test of TC07 did not perform well and TC05 did not fail in an out-of-plane mode. Therefore, there is a lack of comparative results to infer clear conclusions. However, from Fig. 14d it appears that smaller rebar diameters increase the critical tensile strain, since TC05 was close to out-of-plane collapse in the cycle at 0.875% tensile strain, while TC03 failed after 1.125% strain.

## 5 Prediction of experimental results by existing models

The models by Paulay and Priestley (1993) and the adaptation by Parra (2016), Eqs. (1)–(3) in Sect. 1.1, are herein applied to predict the behaviour of each specimen. The geometrical and material properties included in Sect. 2.2 are used. The fixed–fixed boundary conditions of the experiments differ from the original pinned–pinned model hypothesis by Paulay and Priestley (1993), and hence a length of the plastic hinge equal to half of the total test unit height was used, following the approach already proposed by Parra (2016). The results are summarized in Table 5: the model by Paulay and Priestley (1993) provides in general conservative estimates of the critical tensile strain, while the model by Parra (2016) tends to overestimate the experimentally determined critical tensile strain.

Paulay and Priestley (1993) derived the critical tensile strain from equilibrium considerations at maximum out-of-plane displacement, which does not actually correspond to the maximum strain experienced by the member. In fact, neglecting the elastic strain recovery which takes places between the maximum tensile displacement applied and the attainment of maximum out-of-plane displacement leads to an underestimation of the critical tensile strain triggering out-of-plane failure. On the contrary, Parra (2016) accounts for an elastic strain recovery and assumes this value to be equal to 0.5%. This value corresponds roughly to twice the yield strain ($\sim 2\varepsilon_y$), meaning that the reinforcement approximately reached yielding in compression. However, in members with a single layer of reinforcement, as shown in Sect. 4.2, the maximum out-of-plane displacement is attained for low levels of compressive stress. This overestimation of the elastic recovery leads to an overestimation of the critical tensile strains.

## 6 Conclusions

Thin RC walls reinforced with a single layer of longitudinal reinforcement can be vulnerable to out-of-plane instability. Since in Colombia and other South American countries this construction practice is frequently adopted, the present study aims to understand

**Table 5** Comparison between the predictions of the critical tensile strain by existing models and experimental results

| Test units | Predictions | | Experimental | Comparison | |
|---|---|---|---|---|---|
| | $\varepsilon_{cr,PP93}$ (%) | $\varepsilon_{cr,Pa16}$ (%) | $\varepsilon_{cr,exp}$ (%) | $\varepsilon_{cr,exp}/\varepsilon_{cr,PP93}$ | $\varepsilon_{cr,exp}/\varepsilon_{cr,P16}$ |
| TC01 | 0.503 | 1.121 | 0.750–0.875 | 1.49–1.74 | 0.67–0.78 |
| TC02 | 0.202 | 0.749 | 0.500[a] | 2.48 | 0.67 |
| TC03 | 0.603 | 1.244 | 1.000–1.125 | 1.66–1.87 | 0.80–0.90 |
| TC04 | 0.896 | 1.605 | 1.000–1.125 | 1.12–1.26 | 0.62–0.70 |
| TC05 | 0.589 | 1.226 | 1.000[b] | 1.70 | 0.82 |
| TC06 | 0.281 | 0.847 | 0.750–0.875 | 2.67–3.11 | 0.89–1.03 |
| TC07 | 0.362 | 0.947 | –[c] | – | – |
| TC08 | 0.834 | 1.528 | 1.250–1.375 | 1.50–1.65 | 0.82–0.90 |
| TC09 | 0.430 | 1.030 | 0.750–0.875 | 1.74–2.03 | 0.73–0.85 |
| TC10 | 0.434 | 1.035 | 0.625–0.750 | 1.44–1.73 | 0.60–0.72 |
| TC11 | 0.434 | 1.035 | 0.625–0.750 | 1.44–1.73 | 0.60–0.72 |
| TC12 | 0.439 | 1.041 | 0.500–1.000[d] | 1.14–2.28 | 0.48–0.96 |
| | | | Average | 1.67–1.81 | 0.70–0.75 |

$\varepsilon_{cr,PP93}$ critical tensile strain calculated using Eq. (2) by Paulay and Priestley (1993), assuming $l_0 = 0.5 h_{tot}$

$\varepsilon_{cr,Pa16}$ critical tensile strain calculated using Eq. (3) by Parra (2016), assuming $k = 0.5$

$\varepsilon_{cr,exp}$ range of vertical tensile strains triggering out-of-plane failure in the experimental test

[a] The specimen failed within the second cycle at 0.500%

[b] The specimen failed in tension and not due to out-of-plane deformations

[c] The specimen did not fail out-of-plane due to a poor detailing choice

[d] The cycles at 0.0625, 0.625, 0.750 and 0.875% tensile strain were skipped

the specific aspects of this buckling phenomenon. Similarly to previous studies on members with two layers of reinforcement, the boundary element of RC walls was approximated by an equivalent column axially loaded.

Twelve thin RC boundary elements with a single layer of longitudinal reinforcement were tested in tension–compression cycles. The data of the entire experimental program is available for download at DOI 10.5281/zenodo.569799. The specimens developed large lateral deformations, leading to out-of-plane failures. The data collected allowed to obtain insights into the development of out-of-plane instability of boundary elements with a single layer of reinforcement, which are briefly summarised in the following:

(1) The onset of out-of-plane deformations occurs for low values of compression, significantly lower than the yield force of the rebars in compression. Moreover, the measured local strains indicate that the single layer of reinforcement in the crack acts as a hinge around which the parts above and below the crack rotate. These two findings describe the main difference between the instability mechanism of members with one and two layers of reinforcement.

(2) The specimens did not buckle to the same side, even when their geometry was the same. The eccentricity of the single layer of longitudinal reinforcement with regard to the centre line of the section did not seem to have a major influence on the

direction of out-of-plane displacement, while the height above the foundation at which the largest cracks occurred appear to play a significant role.

(3)  It was observed that a critical value of local compressive strain of 0.2% was exceeded in all plastic hinges forming along the test unit height at failure. Therefore, section edge local strains in compression larger than 0.2% in at least three hinges (in the case of fix–fix boundary conditions) represent the critical condition defining the attainment of irrecoverable out-of-plane deformations.

(4)  The crack pattern has a significant influence on the evolution of the out-of-plane instability. The maximum recoverable lateral displacement and the attainment of out-of-plane failure can be explained by a combination of the crack width/spacing in tension and the curvature required to attain limit-state values of local strain.

(5)  Test unit cross-sections with small thickness or large reinforcement content were more prone to out-of-plane instability. The eccentricity of the single layer of reinforcement did not seem to influence the response.

Applicable existing models to calculate the critical tensile strain triggering out-of-plane failure, which were not originally developed for members reinforced with a single layer, were compared with experimental results. The predictions of the critical tensile strains are quite different from the ones obtained in the tests. In particular, the model by Paulay and Priestley (1993) underestimates the experimental results, while the model by Parra (2016) tends to overestimate the critical tensile strain triggering out-of-plane failure.

Future work could include the development of a mechanical model suitable for RC members with a single layer of reinforcement, wherein the progression of lateral instability at low compressive forces and a failure criteria based on the attainment of a limit compressive strain could be accounted for.

# References

Acevedo CE, Creagh A, Moehle JP, et al (2010) Seismic vulnerability of non-special boundary element of shear wall under axial force reversals. Report, Florida International University and University of California, Berkley, USA

Almeida JP, Prodan O, Rosso A, Beyer K (2016) Tests on thin reinforced concrete walls subjected to in-plane and out-of-plane cyclic loading. Earthq Spectra 33:323–345

Arteta CA, Sánchez J, Daza R, et al (2017) Global and local demand limits of thin reinforced concrete structural wall building systems. In: 16th world conference on earthquake engineering. Santiago, Chile

Carrillo J, Alcocer SM, Aperador W (2013) Propiedades mecánicas del concreto para viviendas de bajo costo. Ing Investig y Tecnol 14:285–298

CEB (1978) Model code for concrete structures. Comité Euro International du Béton, Paris

CEN (2004) Eurocode 2: Design of concrete structures—part 1-1: general rules and rules for buildings. European Committee for Standardization, Brussels

Chai YH, Elayer DT (1999) Lateral stability of reinforced concrete columns under axial reversed cyclic tension and compression. ACI Struct J 96:1–10

Chrysanidis TA, Tegos IA (2012) The influence of tension strain of wall ends to their resistance against lateral instability for low-reinforced concrete walls. In: 15th world conference on earthquake engineering. Lisboa, Portugal

Creagh A, Acevedo C, Moehle JP, et al (2010) Seismic performance of concrete special boundary element. Report, University of Texas at Austin and University of California Berkley, USA

Dashti F, Dhakal R, Pampanin S (2017) Blind prediction of the response of a thin singly reinforced concrete flanged wall. Bull Earthq Eng. doi:10.1007/s10518-017-0211-x

FIB (2010) Model code for concrete structures. Fédération Internationale du Béton, Lausanne

González V, Botero JC, Rochel R et al (2005) Propiedades mecánicas del acero de refuerzo utilizado en Colombia. Ing y Cienc 1:67–76

Goodsir WJ (1985) The design of coupled frame-wall structures for seismic actions. PhD Thesis, University of Canterbury, Christchurch, New Zealand

Herrick CK, Kowalsky MJ (2016) Out-of-plane buckling of ductile reinforced structural walls due to in-plane loads. ASCE Struct J 143. doi:10.1061/(ASCE)ST.1943-541X.0001660

Hilson CW, Segura CL, Wallace JW (2014) Experimental study of longitudinal reinforcement buckling in reinforced concrete structural wall boundary elements. In: 10th U.S. national conference on earthquake engineering. Anchorage, Alaska

Mejia LG, Ortiz JC, Osorio G. LI (2004) Housing report—concrete shear wall buildings, report #109. Earthquake Engineering Research Institute (EERI) and International Association for Earthquake Engineering (IAEE), Colombia

Menegon SJ, Wilson JL, Gad EF, Lam NTK (2015) Out-of-plane buckling of limited ductile reinforced concrete walls under cyclic loads. In: 2015 NZSEE conference. Rotorua, New Zealand

Miranda E, Thompson CL, Bertero VV (1990) Cyclic behaviour of shear wall boundary elements incorporating prefabricated welded wire hoops. Report to sponsor Baumann engineering, Earthquake Engineering Research Center, College of Engineering, University of California at Berkley, USA

NDI (2009) Optotrak certus HD, Northern Digital Inc. http://www.ndigital.com/industrial/certushd.php. Waterloo, Ontario, Canada

NSR-10 (2010) Reglamento Colombiano de Construcción Sismo Resistente—Comisión Asesora Permanente para el Règimen de Construcciones Sismo Resistentes. Bogotá D.C., Colombia

Parra PF (2016) Stability of reinforced concrete wall boundaries. PhD Thesis, University of California, Berkeley, USA

Parra PF, Moehle JP (2014) Lateral Buckling in Reinforced Concrete Walls. In: 10th U.S. National conference on earthquake engineering. Anchorage, Alaska

Paulay T, Goodsir WJ (1985) The ductility of structural walls. Bull N Z Natl Soc Earthq Eng 18:250–269

Paulay T, Priestley MJN (1993) Stability of ductile structural walls. ACI Struct J 90:385–392

Rosso A, Almeida JP, Beyer K (2016) Stability of thin reinforced concrete walls under cyclic loads: state-of-the-art and new experimental findings. Bull Earthq Eng 14:455–484

Rosso A, Almeida JP, Beyer K (2017a) Numerical simulation with fibre beam-column models of thin RC columns under cyclic tensile-compressive loading. In: 16th World conference on earthquake engineering. Santiago, Chile

Rosso A, Jimenez-Roa LA, Almeida JP, Beyer K (2017b) Instability of thin single-layered RC walls under cyclic loading: numerical simulation of walls and improved equivalent boundary elements. Submitted to: Finite Elements in Analysis and Design

Rosso A, Jiménez L, Almeida JP, Beyer K (2017c) Experimental campaign on thin RC columns prone to out-of-plane instability: numerical simulation using shell element models. In: VIII Congreso Nacional de Ingeniería Sísmica. Barranquilla, Colombia

Scolari M (2017) Implementation of PARC_CL 2.0 crack model for reinforced concrete members subjected to cyclic and dynamic loading. PhD Thesis, Parma, Italy

SIA (1989) SIA 162, Material tests. Swiss Society of Engineers and Architects, Zurich, Switzerland

Sritharan S, Beyer K, Henry RS et al (2014) Understanding poor seismic performance of concrete walls and design implications. Earthq Spectra 30:307–334

Taleb R, Tani M, Kono S et al (2016) Performance of confined boundary regions of RC walls under cyclic reversal loadings. J Adv Concr Technol 14:108–124

Wallace JW, Massone LM, Bonelli P et al (2012) Damage and implications for seismic design of RC structural wall buildings. Earthq Spectra 28:S281–S299

Welt TS, Massone LM, LaFave JM, et al (2016) Confinement behavior of rectangular reinforced concrete prisms simulating wall boundary elements. ASCE Struct J 318